NANO LETTERS

pubs.acs.org/NanoLett

Plasmonic Nanoparticle Arrays with Nanometer Separation for High-Performance SERS Substrates

Jesse Theiss,[†] Prathamesh Pavaskar,[†] Pierre M. Echternach,[‡] Richard E. Muller,[‡] and Stephen B. Cronin*,[†]

[†]Department of Electrical Engineering, University of Southern California, Los Angeles, California 90089 and [‡]California Institute of Technology, Jet Propulsion Laboratory, Pasadena, California 91109

ABSTRACT We demonstrate a method for fabricating arrays of plasmonic nanoparticles with separations on the order of 1 nm using an angle evaporation technique. Samples fabricated on thin SiN membranes are imaged with high-resolution transmission electron microscopy (HRTEM) to resolve the small separations achieved between nanoparticles. When irradiated with laser light, these nearly touching metal nanoparticles produce extremely high electric field intensities, which result in surface-enhanced Raman spectroscopy (SERS) signals. We quantify these enhancements by depositing a *p*-aminothiophenol dye molecule on the nanoparticle arrays and spatially mapping their Raman intensities using confocal micro-Raman spectroscopy. Our results show significant enhancement when the incident laser is polarized parallel to the axis of the nanoparticle pairs, whereas no enhancement is observed for the perpendicular polarization. These results demonstrate proof-of-principle of this fabrication technique. Finite difference time domain simulations based on HRTEM images predict an electric field intensity enhancement of 82400 at the center of the nanoparticle pair and an electromagnetic SERS enhancement factor of 10^9–10^{10}.

KEYWORDS SERS, plasmonics, nanogap, shadow mask, angle evaporation

Raman spectroscopy is an invaluable tool for many applications. By measuring the precise vibrational energies of molecules, Raman spectroscopy provides a unique signature for chemical identification and differentiation. Its utility is limited, however, by the small Raman scattering cross sections characteristic of most molecules, typically 10^6 times smaller than Rayleigh scattering. The low Raman intensities can be greatly improved through surface-enhanced Raman spectroscopy (SERS). Since its discovery in 1977, hundreds of papers on the subject of SERS have been published.[1] SERS enhancement factors up to 14 orders of magnitude have been reported in the literature.[2,3] Since a vast majority of the previous work in this field has involved roughened metal surfaces and nanoparticles in solution, imaging the exact geometry of the nanoparticle complex was not possible.[4] Furthermore, the number of molecules contributing to a SERS enhanced signal is generally unknown and is usually ascertained through statistical analysis[2,3] and/or a discriminating selection of analyte molecules.[5,6] Consequently, several unexplored experimental factors remain, including the separation between the nanoparticles, the number of nanoparticles within the focal volume, the number of molecules on each nanoparticle, and the extent to which nanoparticles couple plasmonically to each other. Methods for providing reliable SERS substrates, whose parameters can be controlled precisely on the 1 nm scale are much needed and will help bring forth a more complete understanding of SERS and enable new applications of Raman spectroscopy achievable with hand-held spectrometers.

The calculations of Schatz et al., using an interacting dipole model, showed an electric field intensity enhancement factor over 10^6 for the plasmonic resonance between two nearly touching nanoparticles.[7] The electric field enhancement increases sharply for nanoparticle separations below 2 nm. Jiang et al. calculated that two 60 nm diameter spherical Ag nanoparticles separated by 9, 3, and 1 nm produced Raman enhancement factors of 1.5×10^4, 1.7×10^6, and 5.5×10^9, respectively.[8] Numerical finite difference time domain (FDTD) simulations have also shown that coupled nanoparticles produce large electric field enhancements, with SERS enhancement factors up to 10^{10} for a nanoparticle separation of 1 nm.[9] A concurrent and independent chemical mechanism may also contribute to the SERS enhancement due to chemisorption of the analyte molecule to the metal surface. This interaction may produce an intermediate charge-transfer complex with increased Raman scattering cross section or quantum-mechanically alter the electronic states of the analyte molecule.[3,10,11] However, it is generally accepted that this contribution is limited to a few orders of magnitude.[12,13] On the basis of this work, it is now well established that the SERS enhancement, enabling single molecule detection, is dominated by the high electric fields that occur in the small gaps between metal nanoparticles.[7,8,14–16] Several research groups have performed experimental studies of metal nanoparticle dimers

* To whom correspondence should be addressed.
Received for review: 12/16/2009
Published on Web: 07/14/2010

DOI: 10.1021/nl904170g | *Nano Lett.* **2010,** *10,* 2749–2754

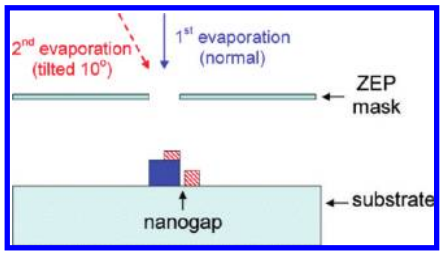

FIGURE 1. Schematic diagram of the angle evaporation technique for fabricating nanometer-size gaps in a controlled manner.

fabricated by standard electron beam lithography. However, the nanoparticle separations in these works were limited by the lithographic techniques to 10−20 nm,[17,18] which is 1 order of magnitude larger than that predicted theoretically to produce significant electric field enhancement. Shadow evaporation is a well-known method for making sub-10-nm gaps between metal structures that has been extensively used for making electrodes, although the feature sizes are generally larger than those of plasmonic nanodevices.[19−21] Angle evaporation was used in conjunction with nanosphere lithography to produce triangular nanoparticles with angle-controlled gaps measured in the range of 4−25 nm.[22] This method limits the shape and size of the particles, which are determined by the hexagonally packed nanosphere mask. The use of a self-assembled monolayer and electron beam lithography can also produce a high yield of 2 nm gaps for nanodevices but contaminates the metal surfaces with a thiolated molecular layer.[23] Other successful methods that can produce molecular-sized gaps include break junctions,[24] electroplating,[25] and electromigration.[26,27] The yield of electromigrated nanogaps has improved significantly, making it a good candidate for the study of SERS phenomena;[28] however, the density is ultimately limited by the electrode geometry. Hence, new methods are desired for controllably creating nanogaps in the range 0.5−2 nm for providing reliable SERS substrates.

Here, we fabricate arrays of metal nanoparticles with separations on the order of 1 nm using electron beam lithography combined with an angle evaporation technique. This work builds on previous research using controlled angled deposition to fabricate nanoscale tunnel junctions used to form single electron transistors[29] and spintronic devices.[30] Figure 1 shows a schematic diagram of the angle evaporation technique. In this scheme, a layer of ZEP-520 electron beam resist is spun on top of a layer of methyl methacrylate (MMA) resist. Since the MMA is more chemically sensitive to electron radiation, electron exposure results in a large undercut by overexposing the more sensitive MMA layer. This leaves a free-standing ZEP mask, as shown schematically in Figure 1. In patterning the nanogaps, a thin layer of metal is first deposited at normal incidence. The sample is then tilted by a small angle (5−10°), and a second layer of metal is deposited. The size of the nanogap is determined by the angle of the second evaporation, θ, and the thickness of the first evaporation, t_1, and is given by t_1 tan θ. Therefore, an angle of $\theta = 10°$ and a thickness of $t_1 = 10$ nm will yield a gap of 1.8 nm. When the angle of evaporation is decreased to $\theta = 5°$, the gap size is reduced to 0.87 nm. We pattern these nanogap structures on thin SiN membranes, which are then imaged using JEOL JEM-2100F high-resolution transmission electron microscopy (HRTEM). HRTEM enables the nanoparticle geometry and gap size to be determined with less than 0.2 nm resolution.

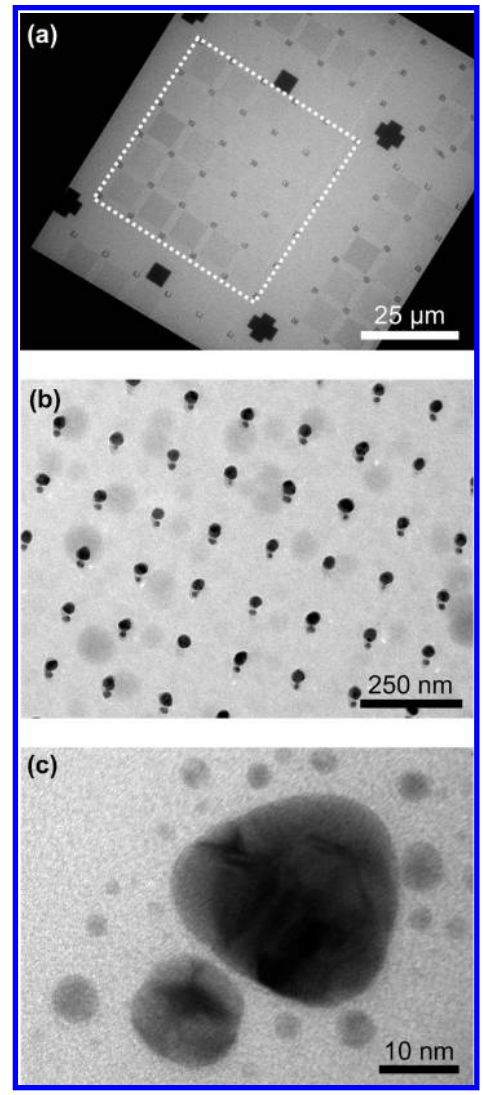

FIGURE 2. (a) Low magnification TEM image of Ag nanoparticle arrays deposited using the angle evaporation technique on a SiN membrane. (b) and (c) High-magnification TEM images of Ag nanoparticle pairs with nanometer-sized gaps.

In this work, a JEOL 9300FSZ electron beam lithography system is used to write 25 sets of nanoparticle arrays, as shown in Figure 2a. Each of these sets covers an approximately 6 μm × 6 μm area and contains a slightly different nanoparticle geometry (i.e., size, shape, separation). A TEM image of one of these arrays is shown in Figure 2b. Figure 2c shows a high-magnification TEM image of one nanoparticle pair with a gap size of 2 nm. This nanoparticle pair (or dimer) was fabricated with $t_1 = 30$ nm and $\theta = 5°$,

DOI: 10.1021/nl904170g | *Nano Lett.* **2010,** *10,* 2749--2754

which is consistent with the trigonometric formula given above ($t_1 \tan \theta$). The second evaporation results in a second nanoparticle that is smaller than that of the first evaporation. This occurs for two reasons. First, the deposition of material tends to close the holes in the lithographic mask. And second, the holes' effective cross sections are decreased at oblique incidence. We estimate a 43.4 % success rate overall for gap formation of the various nanoparticle geometries on our samples. The success rate for these nanogaps depends strongly on the shape and size of the metal particles, as a bridging of two particles in the gap is statistically more probable with a larger overlap region between the two evaporations. Of these successful nanogaps, we measure a gap size of 2.0 ± 0.9 nm.

After fabrication, these silver nanoparticle samples were coated with a non-Raman-resonant dye molecule, *p*-aminothiophenol (p-ATP). The thiol group of the p-ATP molecule has a high affinity for gold and silver surfaces and forms monolayers in dilute solutions followed by rinsing to remove the unbonded molecules. Samples were incubated at room temperature in a 1 mM solution of p-ATP in ethanol for 24 h, rinsed repeatedly with ethanol and deionized water, and then dried with a gentle stream of nitrogen gas. Raman spectra were measured in a Renishaw inVia micro-Raman spectrometer. A 632.8 nm HeNe laser spot is accurately positioned using a high-precision Prior ProScan II microscope stage, which enables spatial mapping of the Raman spectra. The laser was focused to a small Gaussian spot (~0.5 μm diameter) through a 100× objective lens with a numerical aperture of 0.9. A cylindrical lens was inserted in the beam path before the objective lens to spread the laser into an elliptical spot, enabling faster mapping of the Raman intensity across the sample.

The cleanliness of the fabricated silver nanostructures is an important concern due to the confounding spectral peaks that may originate from organic contamination.[31−34] Common treatments such as oxygen plasma or UV ozone to remove lithographic residues are limited because of the highly reactive silver surfaces. In this work, we functionalize the nanoparticles with a p-ATP monolayer immediately after the lift-off process and store them in a vacuum desiccator to protect the nanoparticles from further contamination and degradation. Raman spectra collected on samples without the p-ATP molecules generally show no observable peaks at our experimental laser intensities; however, broad peaks of amorphous carbon were occasionally seen, most notably at higher incident powers. The thermal stability of these delicate, resonant nanostructures is another important concern, given the poor heat sink of the underlying 100 nm silicon nitride membrane.[35] However, no degradation was observed in TEM images taken before and after laser exposure with the powers used in this work (0.88 mW/μm^2). A couple of sites exhibiting moderate to high Raman intensity showed altered spectral profiles, which we attribute to the decomposition of the nearby p-ATP molecules.

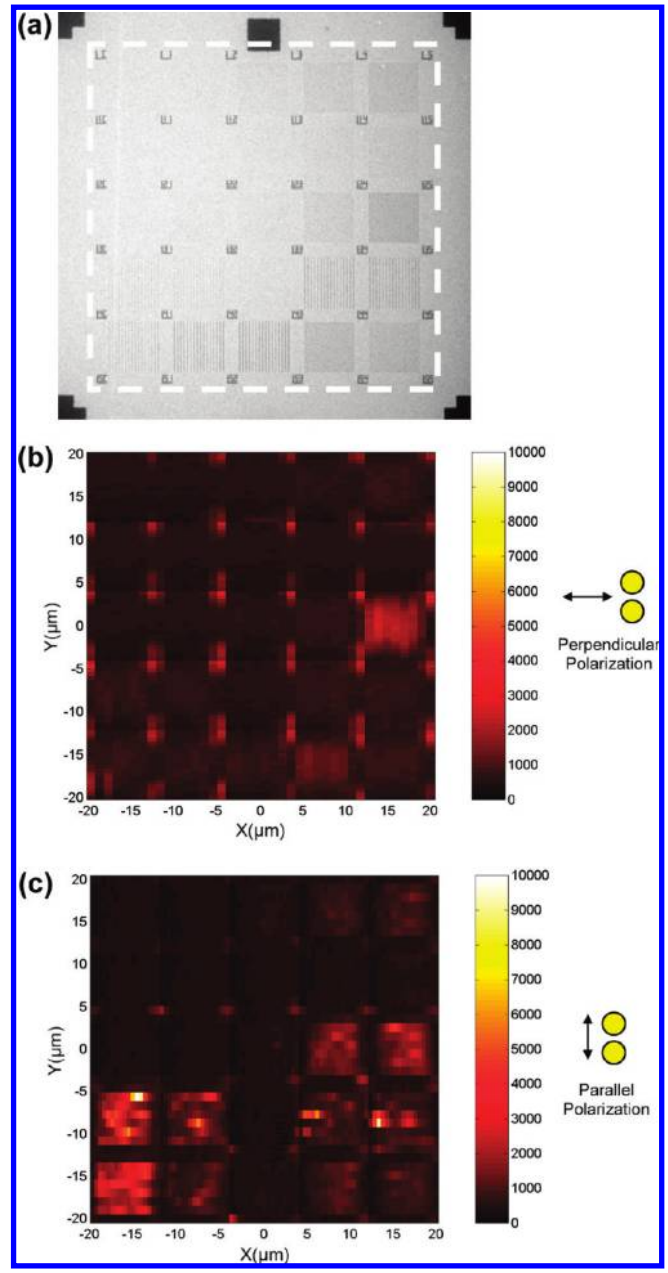

FIGURE 3. (a) TEM image of a 5 × 5 matrix of cells containing different nanoparticle geometries. Spatial mapping with a 632.8 nm laser exciting the 1576 cm^{-1} p-ATP Raman peak across this matrix of various Ag nanoparticle geometries with polarization (b) perpendicular and (c) parallel to the axis of the nanoparticle pairs.

We measure the SERS response of these p-ATP/Ag nanoparticle arrays by spatially mapping their Raman intensities. The Raman intensity is proportional to the fourth power of the electric field $|E|^4$ for small phonon energies and therefore serves as a good measure of the electric field enhancement and relative plasmonic strength. For higher phonon energies, $|E|^4$ still serves as an upper limit to experimental calculations of the SERS electric field enhancement. Parts b and c of Figure 3 show the Raman intensity spatial maps of the 5 × 5 matrix shown in Figure 3a coated with p-ATP, taken with the incident laser polarization oriented perpendicular (Figure

DOI: 10.1021/nl904170g | *Nano Lett.* **2010,** *10,* 2749–2754

3b) and parallel (Figure 3c) to the axis of the nanoparticle pairs.[8,36] A significant increase in the Raman intensity is observed in several nanoparticle cells when the polarization is matched to the angle-evaporated nanometer size gaps, demonstrating the electric field enhancement of the plasmonically coupled nanoparticles. The lack of uniformity in the SERS intensity over these cells is likely due to the inherent sensitivity of the electromagnetic response to the geometry of these nearly touching nanostructures. A small variation in the particle or gap size can result in a large shift in the resonant frequency,[37] pushing the particle off-resonance for a fixed excitation frequency. We believe we may only measure a few fortuitous hotspots that fell within the range of the 632.8 nm laser source. By comparison of the SERS-enhanced cells of Figure 3c with the TEM image of Figure 3a, it is clear that the SERS enhancement does not simply correspond to the metal filling factor of these cells. This further demonstrates the plasmonic nature of this SERS enhancement mechanism, which relies intimately on the plasmonic interaction between adjacent nanoparticles.

On the basis of the TEM image shown in Figure 4a, we can simulate the electromagnetic response of this Ag nanoparticle pair by defining the spatial extent of the metal nanoparticles from this high-resolution TEM image. The x and y dimensions of the particles were determined from the TEM image, while evaporation thicknesses of 15 and 30 nm were used to specify the height of the left and right particle, respectively. FDTD simulations[38] were performed in USC's multiteraflop supercomputing facility, which consists of 5472 CPUs connected by a high-performance, low-latency Myrinet network. Here, full three-dimensional simulations are performed using a grid of 14 million points to discretize the spatial extent of the electric and magnetic fields with up to 2.5 Å resolution in the gap region and carrying out 200000 time steps. The dielectric function we use is based on a fit of the experimental data obtained by Johnson and Christy to a Lorentz−Drude formula.[39] Parts b and c of Figure 4 show the electric field intensity distributions of this silver nanoparticle dimer integrated over the z-dimension, irradiated at normal incidence at the plasmon resonance frequency. For incident light polarized along the axis of the nanoparticle dimer (Figure 4c), the maximum electric field intensity lies in the gap between the nanoparticles, with a value 82400 times that of the incident field intensity at the calculated plasmon resonance occurring at 552 nm. For this nanoparticle pair, the SERS enhancement factor at the most intense point is given by the square of this electric field intensity enhancement factor, giving a value of 6.9×10^9. With polarization perpendicular to the nanoparticle axis, the SERS enhancement factor at the most intense point is calculated to be 6.4×10^4 at this same frequency. Integrating over the area shown in Figure 4c, we find a total SERS enhancement factor of 1.4×10^{11} for parallel polarization. We can also estimate the areal SERS enhancement factor over the area inside the focal volume. On the basis of the

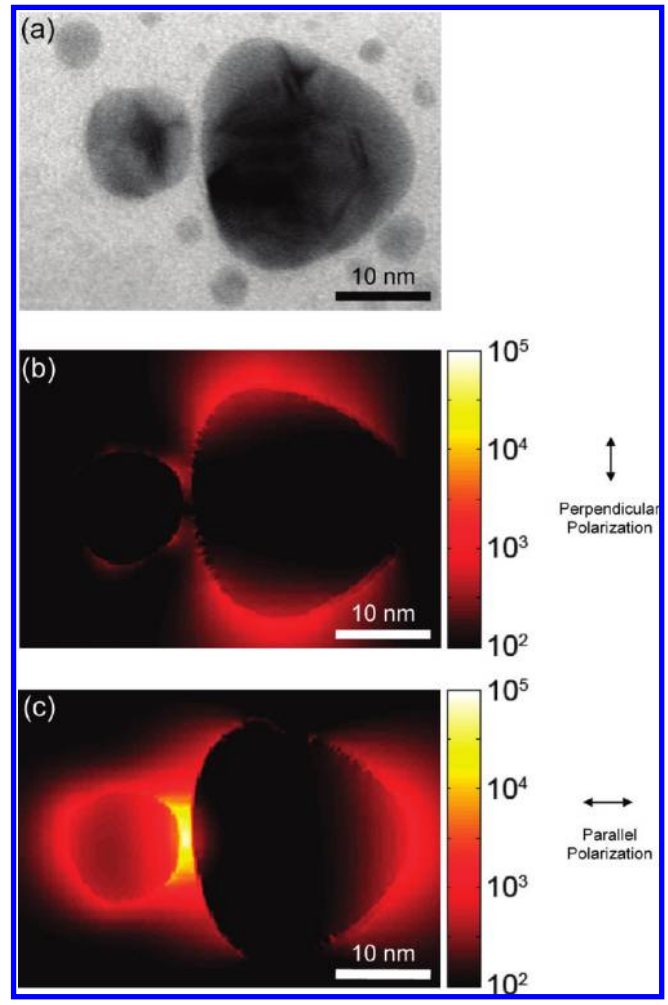

FIGURE 4. (a) TEM image and FDTD simulations of the electric field intensity around a silver nanoparticle dimer with 2 nm separation with incident light polarized (b) perpendicular and (c) parallel to the axis of the nanoparticle pair. The electric field intensity is plotted on a logarithmic scale.

electric field distribution shown in Figure 4b, we calculate the expected areal SERS enhancement by integrating E^4 over the simulation area and then dividing by the incident electric field to the fourth power E_o^4 integrated over the area.

$$\text{areal SERS enhancement factor} = \frac{\int E^4 \, dx \, dy}{\int E_0^4 \, dx \, dy}$$

Following this procedure, we estimate an areal electromagnetic SERS enhancement factor from our FDTD simulation of 5.8×10^3 integrated over a 0.4 μm × 0.4 μm area. The areal EM enhancement factors of our samples are expectedly low due to suboptimal densities of nanoparticle coverage, as seen in Figure 2. From our Raman measurements, it is difficult to quantify the SERS enhancement factor because the number of molecules in the focal volume of the laser spot

DOI: 10.1021/nl904170g | *Nano Lett.* **2010,** *10,* 2749–2754

and in the 2 × 2 nm SERS enhancement volume is unknown. An estimate is made using this SERS enhancement volume from the simulation results and the fact that these signals are collected from multiple nanoparticle pairs within the focal volume. On the basis of the self-assembled monolayer coverage density and the dimensions of our nanoparticles, a SERS EF of 1.1×10^6 is calculated for this particular nanoparticle geometry, as described in detail in the Supporting Information. This experimental EF is over 3 orders of magnitude smaller than the 6.9×10^9 value from our simulations, which may result from exciting the nanoparticle pair slightly off-resonance and overestimating the number of molecules contributing to the measured Raman intensity. Dieringer et al. have developed a method for verifying that there is only one dye molecule in the SERS enhanced Raman spectra using isotopologues of Rhodamine 6G.[40] This enables an accurate measurement of the SERS enhancement factor. This method requires extensive synthesis capabilities and is beyond the scope of the present work.

SERS enhancement is known to arise from two factors, a dominating electromagnetic enhancement and a less significant chemical enhancement, that may work in unison and further complicate our ability to accurately determine the true field enhancement in the nanogaps. The p-ATP molecule has been one of the most commonly studied systems for observing chemical enhancement. One explanation of the chemical enhancement mechanism is a Raman-like process involving charge transfer between metallic energy levels and molecular levels situated around the Fermi level of the metal. These transitions can resonate at specific incident laser energies and also couple vibronically to each other.[41] Experimental and theoretical work into the polarization dependence of the Raman intensity under the chemical mechanism shows differences by a factor of only 5−6× under different polarization and molecular transition moment alignments.[12,41] On the basis of these observations and our simulations, we find our results stem from strong plasmonic coupling between nanoparticle pairs. Our experimental electric field enhancements may be expectedly less due to off-resonance excitation of the nanostructures and an inability to tune the wavelength of the excitation source to the absorption peaks. While most of the gaps produced in this work are larger than 1 nm, quantum mechanical tunneling of electrons between nanoparticles separated by gaps smaller than 1 nm may significantly lower the measured electromagnetic field enhancement and blue-shift the optical absorption.[37] However, our data demonstrate proof-of-principle of SERS enhancement by the plasmonic coupling of nearly touching Ag nanoparticles.

In conclusion, we have demonstrated a method for fabricating nanoparticle pairs with nanometer separations. A significant increase in the Raman intensity is observed when the polarization is matched to the angle-evaporated nanometer size gaps, demonstrating the electric field enhancement of the plasmonically coupled nanoparticles. Numerical simulation of the electromagnetic response of these nanoparticles shows significant enhancements in the calculated electric field and SERS signal, which also depend strongly on the polarization of the incident light. On the basis of the 10^9-10^{10} SERS enhancement factor, these substrates could be used in devices approaching chemical detection at the single molecule level.

Acknowledgment. This research was supported in part by ONR award No. N00014-08-1-0132, AFOSR award No. FA9550-08-1-0019, ARO award No. W911NF-09-1-0240, NSF award No. CBET-0854118, and NASA SURP No. 1346414. Electron beam lithography was performed by Richard E. Muller. This research was partially carried out at the Jet Propulsion Laboratory, California Institute of Technology.

Supporting Information Available. Experimental SERS enhancement factor calculation and gap size statistics. This material is available free of charge via the Internet at http://pubs.acs.org.

REFERENCES AND NOTES

(1) Van Duyne, R. P. *J. Phys. (Paris)* **1977**, *38*, 239–252.
(2) Nie, S.; Emory, S. R. *Science* **1997**, *275* (5303), 1102–1106.
(3) Kneipp, K.; Wang, Y.; Kneipp, H.; Perelman, L. T.; Itzkan, I.; Dasari, R.; Feld, M. S. *Phys. Rev. Lett.* **1997**, *78* (9), 1667–1670.
(4) Camden, J. P.; Dieringer, J. A.; Wang, Y.; Masiello, D. J.; Marks, L. D.; Schatz, G. C.; Van Duyne, R. P. *J. Am. Chem. Soc.* **2008**, *130* (38), 12616–12617.
(5) Dieringer, J. A.; Lettan, R. B.; Scheidt, K. A.; Van Duyne, R. P. *J. Am. Chem. Soc.* **2007**, *129* (51), 16249–16256.
(6) Dieringer, J. A.; Wustholz, K. L.; Masiello, D. J.; Camden, J. P.; Kleinman, S. L.; Schatz, G. C.; Van Duyne, R. P. *J. Am. Chem. Soc.* **2008**, *131* (2), 849–854.
(7) Zou, S. L.; Schatz, G. C. *Chem. Phys. Lett.* **2005**, *403* (1−3), 62–67.
(8) Jiang, J.; Bosnick, K.; Maillard, M.; Brus, L. *J. Phys. Chem. B* **2003**, *107* (37), 9964–9972.
(9) Oubre, C.; Nordlander, P. *J. Phys. Chem. B* **2005**, *109*, 10042.
(10) Campion, A.; Kambhampati, P. *Chem. Soc. Rev.* **1998**, *27* (4), 241–250.
(11) Otto, A.; Mrozek, I.; Grabhorn, H.; Akemann, W. *J. Phys.: Condens. Matter* **1992**, *4*, 1143–1212.
(12) Kambhampati, P.; Child, C. M.; Foster, M. C.; Campion, A. *J. Chem. Phys.* **1998**, *108* (12), 5013–5026.
(13) Doering, W. E.; Nie, S. M. *J. Phys. Chem. B* **2002**, *106* (2), 311–317.
(14) Hicks, E. M.; Zhang, X. Y.; Zou, S. L.; Lyandres, O.; Spears, K. G.; Schatz, G. C.; Van Duyne, R. P. *J. Phys. Chem. B* **2005**, *109* (47), 22351–22358.
(15) Le, F.; Brandl, D. W.; Urzhumov, Y. A.; Wang, H.; Kundu, J.; Halas, N. J.; Aizpurua, J.; Nordlander, P. *ACS Nano* **2008**, *2* (4), 707–718.
(16) Park, S. Y.; Lytton-Jean, A. K. R.; Lee, B.; Weigand, S.; Schatz, G. C.; Mirkin, C. A. *Nature* **2008**, *451* (7178), 553–556.
(17) Atay, T.; Song, J. H.; Nurmikko, A. V. *Nano Lett.* **2004**, *4* (9), 1627–1631.
(18) Su, K. H.; Wei, Q. H.; Zhang, X.; Mock, J. J.; Smith, D. R.; Schultz, S. *Nano Lett.* **2003**, *3* (8), 1087–1090.
(19) Philipp, G.; Weimann, T.; Hinze, P.; Burghard, M.; Weis, J. *Microelectron. Eng.* **1999**, *46* (1−4), 157–160.
(20) Sun, L. F.; Chin, S. N.; Marx, E.; Curtis, K. S.; Greenham, N. C.; Ford, C. J. B. *Nanotechnology* **2005**, *16* (6), 631–634.
(21) Bai, J. G.; Chang, C. L.; Chung, J. H.; Lee, K. H. *Nanotechnology* **2007**, *18* (40), 405307.
(22) Haynes, C. L.; Van Duyne, R. P. *J. Phys. Chem. B* **2001**, *105* (24), 5599–5611.
(23) Negishi, R.; Hasegawa, T.; Terabe, K.; Aono, M.; Ebihara, T.; Tanaka, H.; Ogawa, T. *Appl. Phys. Lett.* **2006**, *88* (22), 223111.

DOI: 10.1021/nl904170g | *Nano Lett.* **2010,** *10,* 2749–2754

(24) Reed, M. A.; Zhou, C.; Muller, C. J.; Burgin, T. P.; Tour, J. M. *Science* **1997**, *278* (5336), 252–254.
(25) Morpurgo, A. F.; Marcus, C. M.; Robinson, D. B. *Appl. Phys. Lett.* **1999**, *74* (14), 2084–2086.
(26) Park, H.; Lim, A. K. L.; Alivisatos, A. P.; Park, J.; McEuen, P. L. *Appl. Phys. Lett.* **1999**, *75* (2), 301–303.
(27) Park, J.; Pasupathy, A. N.; Goldsmith, J. I.; Chang, C.; Yaish, Y.; Petta, J. R.; Rinkoski, M.; Sethna, J. P.; Abruna, H. D.; McEuen, P. L.; Ralph, D. C. *Nature* **2002**, *417* (6890), 722–725.
(28) Ward, D. R.; Grady, N. K.; Levin, C. S.; Halas, N. J.; Wu, Y. P.; Nordlander, P.; Natelson, D. *Nano Lett.* **2007**, *7* (5), 1396–1400.
(29) Schneiderman, J. F.; Delsing, P.; Shaw, M. D.; Bozler, H. M.; Echternach, P. M. *Appl. Phys. Lett.* **2006**, *88* (8), 3.
(30) Valenzuela, S. O.; Tinkham, M. *Appl. Phys. Lett.* **2004**, *85* (24), 5914–5916.
(31) Kudelski, A.; Pettinger, B. *Chem. Phys. Lett.* **2000**, *321* (5−6), 356–362.
(32) Domke, K. F.; Zhang, D.; Pettinger, B. *J. Phys. Chem. C* **2007**, *111* (24), 8611–8616.
(33) Otto, A. *J. Raman Spectrosc.* **2002**, *33* (8), 593–598.
(34) Richards, D.; Milner, R. G.; Huang, F.; Festy, F. *J. Raman Spectrosc.* **2003**, *34* (9), 663–667.
(35) Schuck, P. J.; Fromm, D. P.; Sundaramurthy, A.; Kino, G. S.; Moerner, W. E. *Phys. Rev. Lett.* **2005**, *94* (1), No. 017402.
(36) Baia, M.; Toderas, F.; Baia, L.; Popp, J.; Astilean, S. *Chem. Phys. Lett.* **2006**, *422* (1−3), 127–132.
(37) Zuloaga, J.; Prodan, E.; Nordlander, P. *Nano Lett.* **2009**, *9* (2), 887–891.
(38) Taflove, A.; Hagness, S. C. *Computational electrodynamics: the finite-difference time-domain method*, 3rd ed.; Artech House: Boston, MA, 2005.
(39) Johnson, P. B.; Christy, R. W. *Phys. Rev. B* **1972**, *6* (12), 4370–4379.
(40) Dieringer, J. A.; Lettan, R. B.; Scheidt, K. A.; Duyne, R. P. V. *J. Am. Chem. Soc.* **2007**, *129*, 16249.
(41) Lombardi, J. R.; Birke, R. L. *J. Phys. Chem. C* **2008**, *112* (14), 5605–5617.

DOI: 10.1021/nl904170g | *Nano Lett.* **2010,** *10,* 2749--2754